Supporting Information

Tuning thermoelectric performance of π-d conjugated nickel coordination polymers through metal−ligand frontier molecular orbital alignment

Xue Yong[a], Wen Shi[a], Gang Wu[a], Shermin S. Goh[b], Shiqiang Bai[b], Jian-Wei Xu[b], Jian-Sheng Wang[c] and Shuo-Wang Yang[a]*

[a.] *Institute of High Performance Computing, Agency for Science, Technology and Research, 1 Fusionopolis Way, #16-16 Connexis, Singapore 138632. *E-mail: yangsw@ihpc.a-star.edu.sg; Tel: +65 64191343*
[b.] *Institute of Materials Research and Engineering, Agency for Science, Technology and Research, 2 Fusionopolis Way, Singapore 138634*
[c.] *Department of Physics, National University of Singapore, Singapore 117551*

Table of Contents

Section I. Polymer backbone geometric structures

We first optimized the pentamer of poly(Ni-benzene-1,2,4,5-tetrathiolate) (Fig. S1) using M06 exchange-correlation functional[1] implemented in Gaussian 16 program[2] with SDD basis set (with the SDD effective core potential)[3] for Ni atoms and 6-311+G(d,p) basis set for other atoms. The optimized pentamer is found to be a planner with no imaginary frequency. The Ni-Ni distance is found to be 8.41 Å, which is consistent with a previous study using B3LYP functional.[4]

Four different exchange-correlation functionals, that is LDA[5]+U (U = 6.0 eV)[5] with Grimme's DFT-D3 corrections, PBE[6] with Grimme's DFT-D3 corrections (PBED), PBE+U (U = 6.0 eV) with Grimme's DFT-D3 corrections and HSE06[7] with Grimme's DFT-D3 corrections, have been tested to optimize the polymer structure of poly(Ni-benzene-1,2,4,5-tetrathiolate) implemented in VASP package, and the influence of different functionals is negligible (Table S1). The lattice parameters from PBED (8.41 Å) and PBE+U (8.41 Å) are close to the B3LYP results for the Ni-Ni distance in pentamer (8.41 Å). The Ni-S bond from PBED (2.14 Å) and HSE06 (2.14 Å) are close to the experimental values (2.15 Å).[8] The other bond lengths were not given in the experimental work, so we do not have direct comparison with experimental values. Considering the accuracy and computational cost, PBED functional was utilized for geometry optimization thereafter.

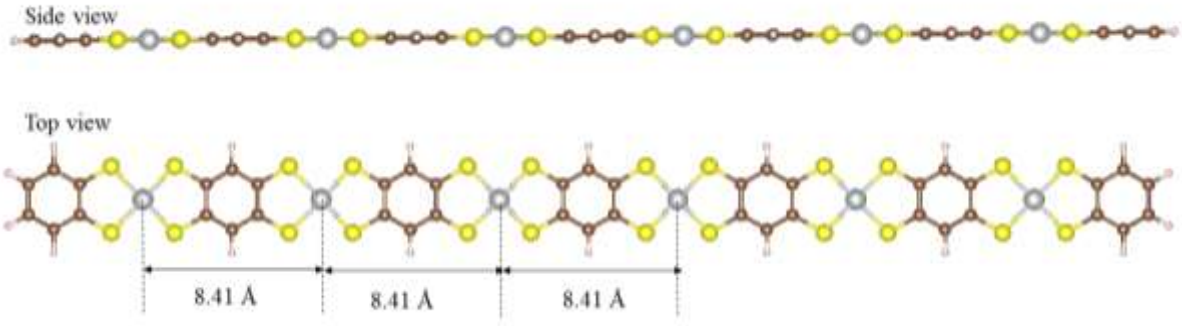

Fig. S1. The side (up) and top (down) views of optimized pentamer for poly(Ni-benzene-1,2,4,5-tetrathiolate) by Gaussian 16 program[2] at M06 level. The distance of two nearest neighboring nickel atoms is shown in the figure. The SDD basis set was used for nickel atoms, and the 6-

31G(d,p) basis set for other atoms. C, S, Ni, and H atoms are represented in grey, yellow, blue and white, respectively.

Table S1. Selected bond lengths (unit Å) for **Ni-ETT**, **Ni-BTT**, **Ni-DMBTT**, **Ni-DNBTT**, **Ni-BQTT**, and ***z*-Ni-BTT.**

		a	Ni-S	S-C	C-C(1)	C-C(2)	Delta[a]
Ni-BTT	LDA+U	8.27	2.10	1.69	1.43	1.39	0.04
	PBE+U	8.41	2.16	1.70	1.46	1.40	0.06
	PBED	8.41	2.14	1.71	1.44	1.40	0.04
	HSE06	8.38	2.14	1.71	1.44	1.39	0.05
	Exp.		2.15				
Ni-ETT[b]		5.96	2.15	1.696	1.44		
Ni-DMBTT[b]		8.42	2.14	1.71	1.44	1.40	0.04
Ni-DNBTT[b]		8.42	2.14	1.71	1.44	1.40	0.04
Ni-BQTT[b]		8.41	2.14	1.69	1.40	1.49	0.09
***z*-Ni-BTT**[b]		14.62	2.13	1.71	1.42	1.43	

[a], delta: C-C (1): fuse-linking, C-C(2): bridge-linking, bond(C-C(1))-bond(C-C(2)), [b] computed with PBED

Section II. Electronic structure characteristics

Different functionals including LDA+U (U = 6.0 eV), PBE, PBE+U (U = 6.0 eV), B3LYP[3] and HSE06 have been used for the band structure calculations of poly(Ni-benzene-1,2,4,5-tetrathiolate). LDA+U, PBE, and PBE+U results are analogous which show a metallic band structure (Fig. S2). However, the results are not consistent with the experimental observation of the oligomer of Ni-dithiolene complexes, which were found to possess a narrow bandgap (0.63 eV)[9] using optical spectroscopy technique. The bandgap of the polymer should be smaller than 0.63 eV due to a higher degree of electron delocalization as compared to the oligomer. In fact, the B3LYP and HSE06 find poly(Ni-benzene-1,2,4,5-tetrathiolate) is a semiconductor with a small band gap of around 0.08 eV. The band profiles calculated by PBE+U (U = 6.0 eV), B3LYP and HSE06 functional are nearly the same. Herein the HSE06 exchange-correlation functional was used to conduct the electronic structure calculations.

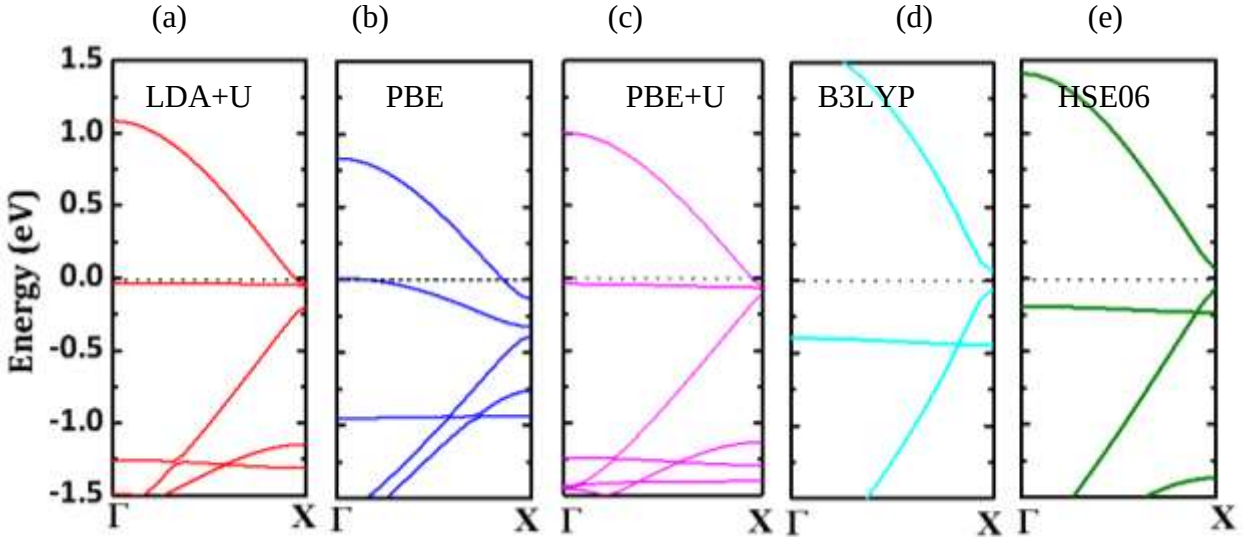

Fig. S2. Band structures of **Ni-BTT** calculated by (a) LDA+U (6.0 eV),[12] (b) PBED,[5] (c) PBE+U (U = 6.0 eV),[7] (d) B3LYP,[1] and (e) HSE06,[8]. The band energies are shifted relative to the Fermi energy level highlighted in the horizontal red dashed line. The reciprocal coordinates of high-symmetry k-points in the first Brillouin zone are Γ = (0, 0, 0) and X = (0.5, 0, 0). The black dotted lines represent the fermi level.

Spin-polarized and non-spin polarized calculations were performed using HSE06 functional 2×1×1 supercells to elaborate the magnetic properties. The ferromagnetic (FM) and anti-ferromagnetic (AFM) states are considered with the initial spin on Ni atoms. The energy of AFM, FM, and non-magnetic (NOM) states are found to be close with energy differences smaller than 0.035 eV/cell (Fig. S3). The spin-up and spin-down bands display small split in the band structures for AFM and FM states (Fig. S3). In addition, the magnetic momentum of Ni in FM and AFM are found to as low as 0.36 and 0.00 μ_B/ Ni. These low energy difference and small magnetic moments suggest that **Ni-BTT** is not likely to be magnetic at temperatures of 300 K and above.[10]

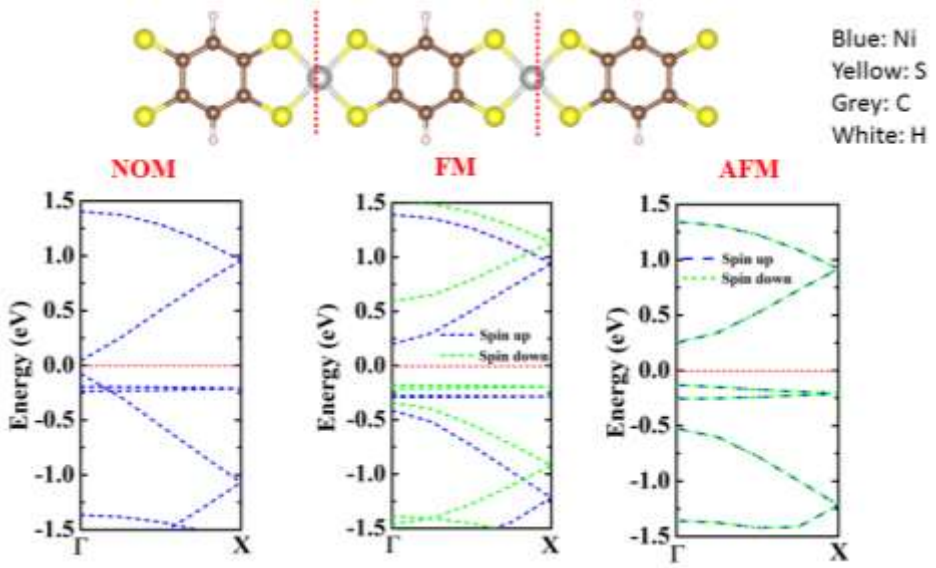

Total energy	non-magnetic (NOM)	ferromagnetic (FM)	anti-ferromagnetic (AFM)	E_{FM}-E_{NOM}	E_{AFM}-E_{NOM}
ev/cell	-98.613	-98.648	-98.630	-0.035	-0.017
ev/atom	-7.586	-7.588	-7.587	-0.002	-0.001
Moments (/Ni)		0.36	0.00		

Fig. S3. The structure (top), band-structures (middle), and the total energies for the non-magnetic (NOM), ferromagnetic (FM), and anti-ferromagnetic (AFM) states of **Ni-BTT**.

Table S2. The valence and conduction band bandwidths, VBM (E_{VBM}) and CBM (E_{CBM}) energy levels and band gap (E_g) of **Ni-ETT**, **Ni-BTT**, **Ni-DMBTT**, **Ni-DNBTT**, **Ni-BQTT**, and ***z*-Ni-BTT.**

	VB-bandwidth (eV)	CB-bandwidth (eV)	E_{VBM} (eV)	E_{CBM} (eV)	E_g (eV)
Ni-ETT	1.80	1.36	-5.27	-4.22	1.05
Ni-BTT	1.78	1.37	-5.63	-5.55	0.08
Ni-DMBTT	1.75	1.36	-5.37	-5.29	0.08
Ni-DNBTT	1.68	1.40	-6.57	-6.47	0.10
Ni-BQTT	0.78	0.80	-6.42	-5.64	0.78
***z*-Ni-BTT**	0.14	0.23	-5.18	-4.44	0.74

Table S3. Bader charge (unit: *e* per atom/group)

	Ni	S	aromatic-ring	Functional group
Ni-ETT	0.49	0.07	-0.72	
Ni-BTT	0.52	0.05	-0.37	
Ni-DMBTT	0.53	0.06	-0.44	0.21
Ni-DNBTT	0.58	0.03	0.27	-0.47
Ni-BQTT	0.50	0.07	1.28	-1.04
***z*-Ni-BTT**	0.54	0.01/-0.02	-0.71	

Bader charge indicates that -CH_3 lose 0.21 *e* to the spacer while -NO_2 group gains 0.47 *e* to the spacer, which characterize the electron-donating/withdrawing ability of -CH_3/-NO_2 groups.

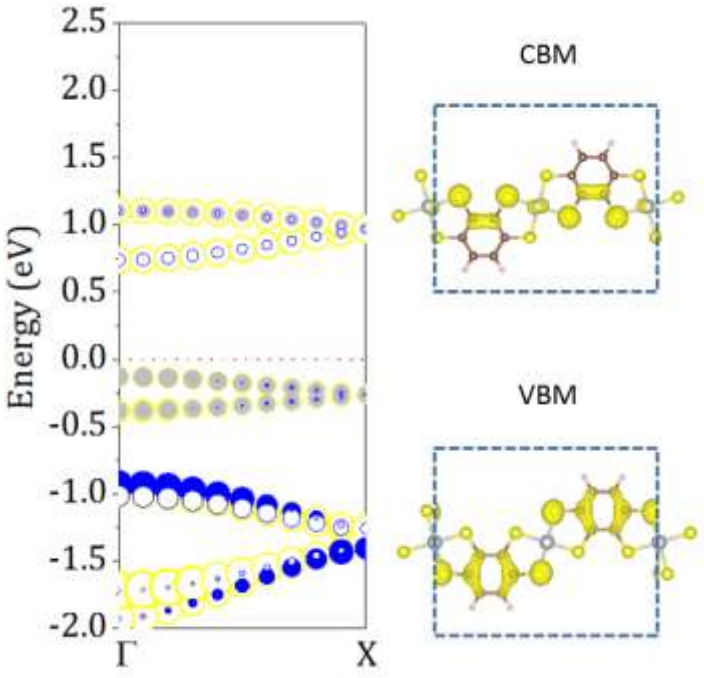

Fig. S4. The band structure and partial charge density of the VBM and CBM states of ***z*-Ni-BTT**.

Section III. Electron-phonon coupling characteristics and intrinsic mobility prediction

Bardeen and Shockley provided us with a simple criterion to confirm the dominant role of an acoustic phonon in the charge transport process.[11] They proposed that at room temperature, the electron energy is around k_BT, namely 26 meV. Its velocity can be derived to be 10^5 m s^{-1}. Thus its de Broglie wavelength is about 70 Å. The energy of a phonon of the corresponding wavelength is about 2 meV, which is the acoustic phonon. So the electron is scattered elastically mainly by the acoustic phonons near room temperature. From the phonon dispersion of **Ni-BTT** (Fig. S5), we can clearly find that the optical branches with the lowest energy are located around 5 meV, which is higher than 2 meV, such that optical branches cannot scatter the electron effectively. Accordingly, in this work, the acoustic phonon scatterings are taken into account using deformation potential (DP) theory.

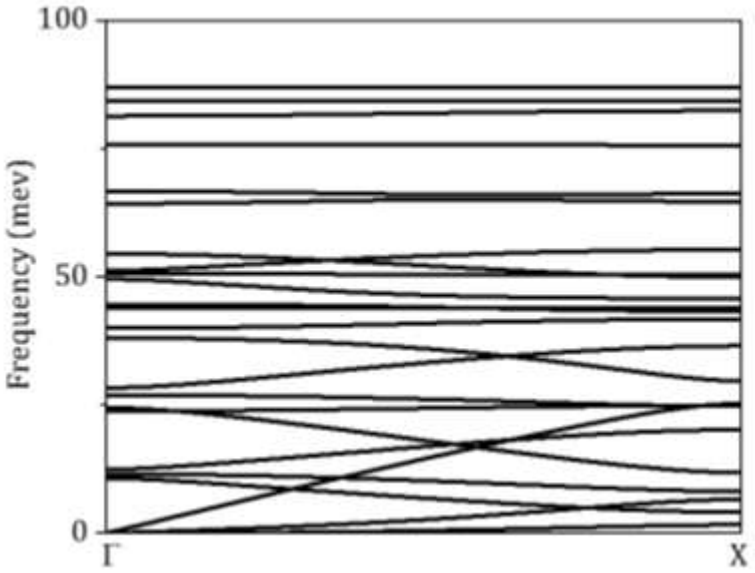

Fig. S5. Phonon dispersion for the isolated **Ni-BTT** chain.

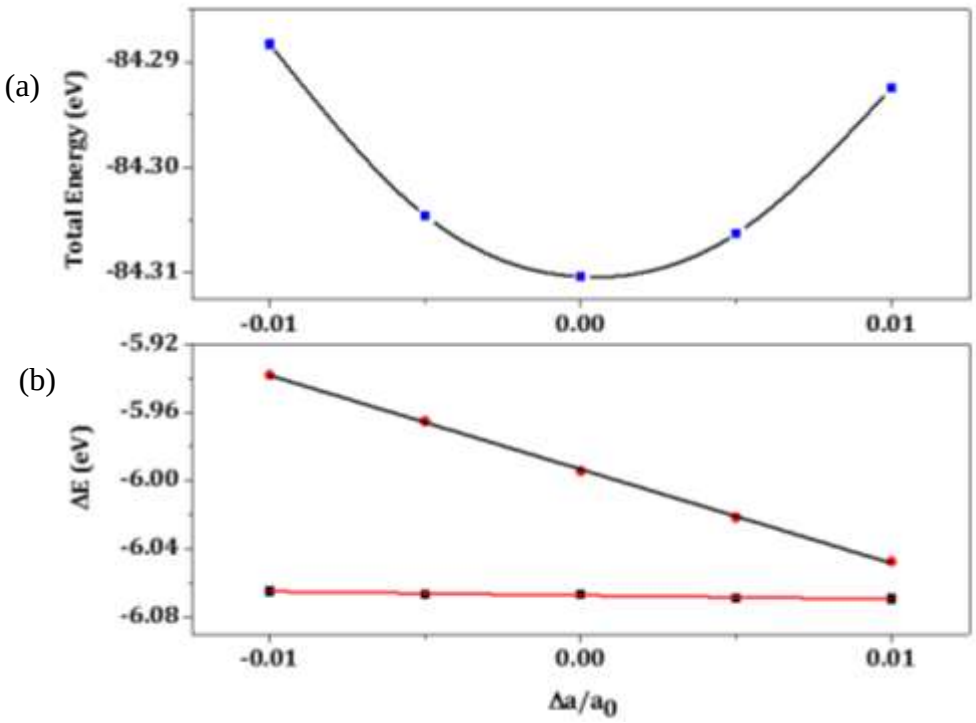

Fig. S6. (a) The total energy with respect to dilations for **Ni-BTT** in the crystal axis *x* direction. The solid black lines are the parabolic fittings of data points. (b) The band energy shifts concerning dilations for **Ni-BTT** in the crystal axis *x* direction. The valence band maximum (VBM) (red) and conduction band minimum (CBM) (black) are used to obtain the DP constants of holes and electrons, respectively. The energies are all calibrated with the vacuum level during the lattice deformations. The solid lines are the linear fittings of data points.

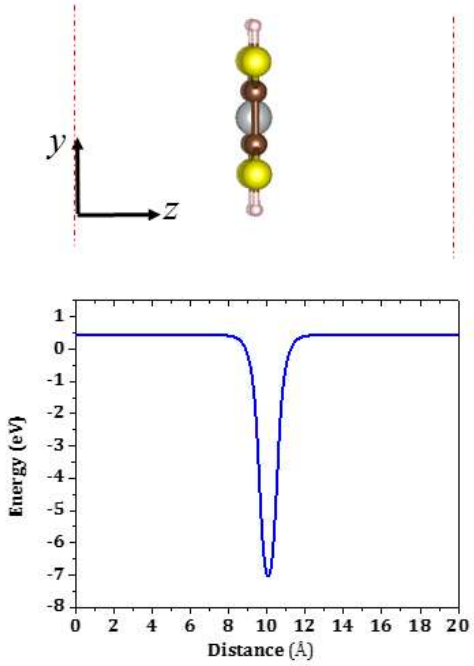

Fig. S7. The schematic illustration of the calibration method: the electrostatic potential profiles for **Ni-BTT** in the crystal axis *z* direction.

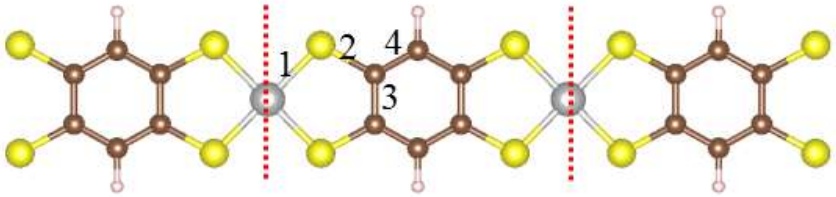

1: Ni-S, 2: S-C, 3: C-C(1), 4 C-C(2)

	Ni-S	S-C	C-C(1)	C-C(2)	C-func
Ni-ETT	0.5893	0.1627	0.1032		
Ni-BTT	0.5585	0.31683	0.00631	0.26542	
Ni-DMBTT	0.6066	0.308305	0.01964	0.24937	0.02315
Ni-DNBTT	0.6133	0.27188	0.02379	0.21378	0.07633
Ni-BQTT	0.51403	0.2954	0.02911	0.3913	0.06732
***z*-Ni-BTT**	0.59775/0.14773	0.20677/0.05092	0.14039	0.3444/0.0587	

Fig. S8. The numbering scheme for the selected bond in the coordination polymer and the bond deformation in CPs when the lattice is under a 1% percent structural deformation. In the last row, the value on the left of "/" corresponding the bonds with para-S and C atoms, while the value on the right of "/" is the value for the bonds involved ortho- S and C atoms.

Table S4. The computed room-temperature optimal doping concentration, power factor, Seebeck coefficient, conductivity, relaxation time, and elastic constant for the p-type performance of **Ni-ETT**, **Ni-BTT**, **Ni-DMBTT**, **Ni-DNBTT**, **Ni-BQTT**, and ***z*-Ni-BTT**. The values are given for the corresponding doping carrier concentration in the second column.

	N_{opt} (10^{20} cm^{-3})	$(S^2\sigma)_{max}$ (10^5 μWm^{-1}K^{-2})	S (μV K^{-1})	σ (10^5 S cm^{-1})	μ (cm^2 V^{-1} s^{-1})	τ (fs)	E_1 (eV)	C_{ii} (10^{-7} J m^{-1})
Ni-ETT	8.88	3	214	1.17	840	40	4.45	1.18
Ni-BTT	0.30	3032	199	767.00	1.28X10^7	487881	0.12	1.52
Ni-DMBTT	1.61	103	193	27.71	9.08x10^4	4441	0.29	1.57
Ni-DNBTT	0.39	25	179	7.50	9.98x10^4	4945	1.04	1.34
Ni-BQTT	4.60	577	183	173.39	2.53x10^5	43531	0.24	1.49
***z*-Ni-BTT**	8.35	1	206	0.29	219	122	1.28	0.80

Section IV. Carrier concentration dependent TE properties prediction

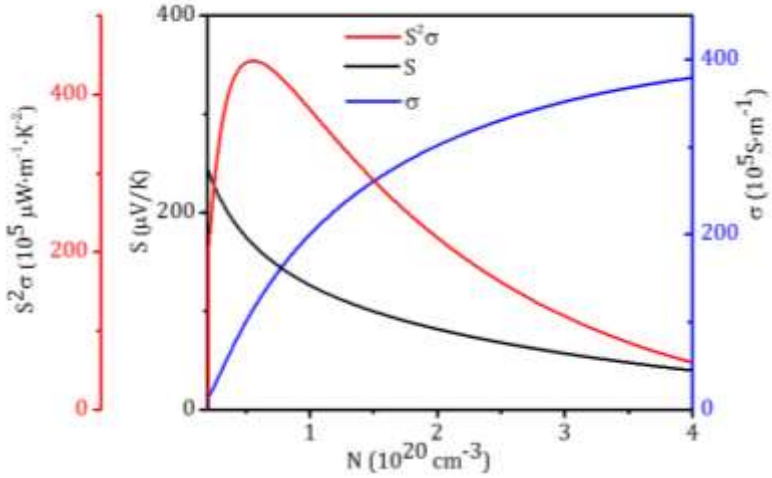

Fig. S9. Variation of Seebeck coefficient, conductivity, and power factor with different carrier concentration for **Ni-BTT** at room temperature.

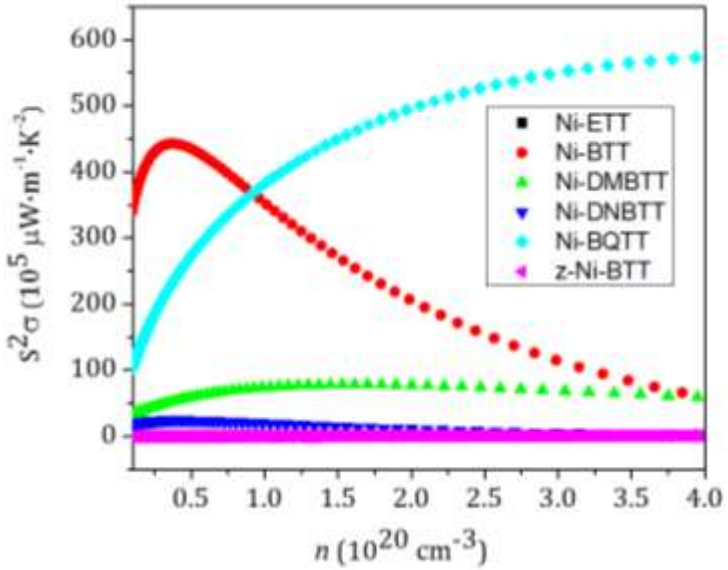

Fig. S10. Variation of power factor with carrier concentration below 10^{20} cm^{-3} for **Ni-ETT**, **Ni-BTT**, **Ni-DMBTT**, **Ni-DNBTT**, **Ni-BQTT**, and ***z*-Ni-BTT**, respectively at room temperature.

Table S5. The computed room-temperature optimal doping concentration, power factor, Seebeck coefficient, conductivity, relaxation time, and elastic constant for the n-type performance of **Ni-ETT**, **Ni-BTT**, **Ni-DMBTT**, **Ni-DNBTT**, **Ni-BQTT**, and ***z*-Ni-BTT** at room temperature. The values are given for the corresponding doping carrier concentration in the second column.

	N_{opt} (10^{20} cm^{-3})	$(S^2\sigma)_{max}$ (10^5 μ W m^{-1} K^{-2})	S (μV K^{-1})	σ (10^5 S cm^{-1})	E_1 (eV)	C_{ii} (10^{-7} J m^{-1})
Ni-ETT	9.90	15.0	-160	5.52	2.25	1.18
Ni-BTT	11.10	1.0	-59	3.66	5.45	1.52
Ni-DMBTT	10.61	0.9	-51	3.39	5.86	1.57
Ni-DNBTT	10.00	1.0	-54	3.03	4.69	1.34
Ni-BQTT	4.39	3.0	-186	0.94	3.29	1.49
z-Ni-BTT	9.97	0.7	-170	0.2	2.50	0.8

Section V. References

1 Y. Zhao and D. G. Truhlar, *Theor. Chem. Acc.*, 2008, **120**, 215–241.

2 D. J. Gaussian 16,Frisch, M. J.; Trucks, G. W.; Schlegel, H. B.; Scuseria, G. E.; Robb, M. A.; Cheeseman, J. R.; Scalmani, G.; Barone, V.; Petersson, G. A.; Nakatsuji, H.; Li, X.; Caricato, M.; Marenich, A. V.; Bloino, J.; Janesko, B. G.; Gomperts, R.; Mennucci, 2016.

3 M. Dolg, U. Wedig, H. Stoll and H. Preuss, *J. Chem. Phys.*, 1987, **86**, 866–872.

4 R. Matsuoka, R. Sakamoto, T. Kambe, K. Takada, T. Kusamoto and H. Nishihara, *Chem. Commun.*, 2014, **50**, 8137–8139.

5 J. P. Perdew and A. Zunger, *Phys. Rev. B*, 1981, **23**, 5048–5079.

6 J. P. Perdew, K. Burke and M. Ernzerhof, *Phys. Rev. Lett.*, 1996, **77**, 3865–3868.

7 J. Heyd, G. E. Scuseria and M. Ernzerhof, *J. Chem. Phys.*, 2003, **118**, 8207–8215.

8 J. Ochocki, P. Chaudhuri, W. L. Driessen, R. A. G. De Graaf, F. B. Hulsbergen and J. Reedijk, *Inorganica Chim. Acta*, 1990, **167**, 15–20.

9 B. Liu, W. Qiao and Z. Y. Wang, *RSC Adv.*, 2015, **5**, 6815–6822.

10 D. Parker, A. F. May, H. Wang, M. A. McGuire, B. C. Sales and D. J. Singh, *Phys. Rev. B - Condens. Matter Mater. Phys.*, 2013, **87**, 1–8.

11 J. Bardeen and W. Shockley, *Phys. Rev.*, 1950, **80**, 72–80.